ORIGINAL ARTICLE

Numerical analysis of the behavior of beam-column precast connections without continuity reinforcement

Análise numérica do comportamento de ligações viga-pilar pré-moldadas sem armadura de continuidade

João Victor Maciel de Andrade Silva[a] (iD)
Leandro Vanalli[b] (iD)
Luiz Antonio Farani de Souza[c] (iD)
Caio Prestupa Malta Rolim[b] (iD)

[a]Universidade Estadual de Mato Grosso do Sul – UEMS, Coordenação de Engenharia Ambiental e Sanitária, Dourados, MS, Brasil
[b]Universidade Estadual de Maringá – UEM, Departamento de Tecnologia, Umuarama, PR, Brasil
[c]Universidade Tecnológica Federal do Paraná – UTFPR, Coordenação de Engenharia Civil, Apucarana, PR, Brasil

Abstract: In this paper, the behavior of four beam-column connections in precast structures, without continuity reinforcement, subjected to negative bending moment was analyzed through numerical simulation using the ABAQUS®, which is based on the Finite Element Method. Nonlinear analysis was performed initially with calibration using an experimental model found in the literature. The analysis showed that the filling of the beam-pillar interfaces with rigid material allows for greater stiffness and bond strength, exhibiting a secant rotational flexural stiffness at the beginning of the yield of the anchor at least 5.5 times greater than in models without filling. There are benefits in considering the rotational stiffness of this type of connection in precast single-storey or small height structures in relation to their stress distribution that provide greater competitiveness to precast structures.

Keywords: finite element, ABAQUS, deformability, semi-stiffness.

Resumo: Nesta pesquisa foi analisado o comportamento de quatro modelos de ligações viga-pilar em estruturas pré-moldadas, sem armadura de continuidade, submetidas a momento fletor negativo por meio de simulação numérica com a utilização do programa ABAQUS®, o qual é baseado no Método dos Elementos Finitos. A análise mostrou que o preenchimento das interfaces viga-pilar com material rígido proporciona maior rigidez e resistência à ligação, exibindo rigidez rotacional secante ao início do escoamento do chumbador pelo menos 5,5 vezes maior que em modelos sem o preenchimento. Considerar a rigidez desse tipo de ligação em projetos de estruturas pré-moldadas de um pavimento ou de pequena altura permite benefícios na distribuição de esforços das mesmas tornando-as mais competitivas.

Palavras-chave: elementos finitos, ABAQUS, deformabilidade, semirrigidez.

1 INTRODUCTION

Precast structures are of great importance for the modernization process of civil construction, as their characteristics present great benefits, such as reduced input waste, technological innovation, increased yield, and reduced construction time, as reported by El Debs [1].

Recently, precast structures have had their use expanded with the social and technological development of Brazil. They have a wide range of applications, from buildings to large works of art and infrastructure. In buildings, precast structures can be used both in single-storey buildings (warehouses, halls, and event centers) and multi-storey buildings.

With the greater application of precast structures in civil constructions, there is an increasing need for research and development activities on the subject. In this sense, it is essential to understand how their connections work. Kataoka et al. [2] state that the main difference between precast structures and reinforced concrete structures cast on site is the presence of connections, and according to Lacerda et al. [3] connections are fundamental to the behavior of precast structures.

In recent years, much research has been carried out to conceive connections with high levels of stiffness at the bending moment, mainly for application in tall structures, which are under greater horizontal stresses and harder to stabilize, such as the research by Baldissera [4] and El Debs et al. [5]. Oliveira Júnior et al. [6], also looking for a connection with high stiffness, proposed the use of concrete with the incorporation of steel fibers for infrastructure works. More recently Lacerda et al. [3] evaluated the influence of grout filling of beam-column interfaces in connections with continuity reinforcement, and they observed an increase in the stiffness and resistance of the filled connections.

However, these stiffer connections, in general, are obtained through concrete cast at the site, in the region of the connection, prestressing, or welded metal sheets. The execution of connections with these characteristics reduces the speed of construction, which is one of the main advantages of precast concrete according to El Debs [1].

It should be noted that precast structures can also be applied in single-storey buildings and small buildings (up to 12 m high according to El Debs [1]). These types of buildings need less stiffness in their connections, given the lower intensity of horizontal stresses; in these cases, it is more interesting to use simple connections, which allow greater yield and speed in construction.

Sawasaki [7] conducted an experimental and numerical study of connections without continuity reinforcement, formed by anchor and bearing pad, for application in small buildings and warehouses. The connections showed low stiffness, however, the influence on the stress distribution in the structures was positive, with a reduction of up to 47.9% of the bending moment at the base of the columns.

In this context, this article presents a comparative analysis of the behavior of four different precast connections without continuity reinforcement. The analyzed connections are easy to implement and are basically formed by a corbel with anchor and bearing pad for beam connection with a half-joint.

The analysis was carried out by numerical simulation, with physical and geometric nonlinearity, using the computer program ABAQUS® based on the Finite Element Method (FEM). It considered the nonlinear behavior of concrete, reinforcement, and anchor. For concrete, the constitutive model 'Concrete Damaged Plasticity' (CDP) was used and for reinforcement, ideal elastoplastic behavior was used. The solution of the nonlinear problem was obtained using the Newton-Raphson method, in an incremental and iterative design.

2 ANALYSIS METHODOLOGY

For calibrating the numerical analysis, a simulation was carried out of the connection model analyzed experimentally by Miotto [8]. This connection is made by means of a corbel with an anchor and modified mortar pad (MMP). The connection has superior continuity reinforcement, next to the concrete topping of the precast slab and can be seen in Figure 1. This connection was chosen because it presents reliable results, in addition to having a vast description of all experimental steps. Another important factor for choosing this connection was its complexity, which displays several components and characteristics relevant to this research, which can be calibrated and later extrapolated for analysis in other models.
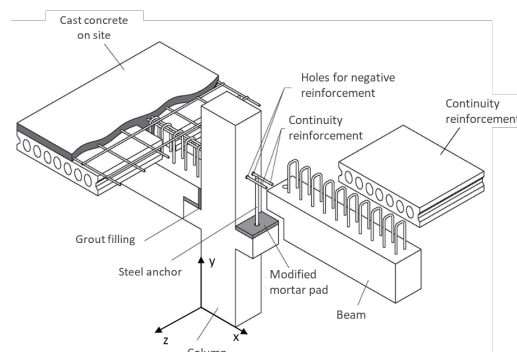

Figure 1. Calibration connection (Adapted from El Debs [1]).

In this context, the moment-rotation curve, the failure mode, the cracking and ultimate moments, and the cracking pattern were analyzed in the numerical model. From the calibration model, four connection models without continuity reinforcement and with different characteristics were proposed. All models are derived from a cross-shaped, central column connection with dimensions as shown in Figure 2.
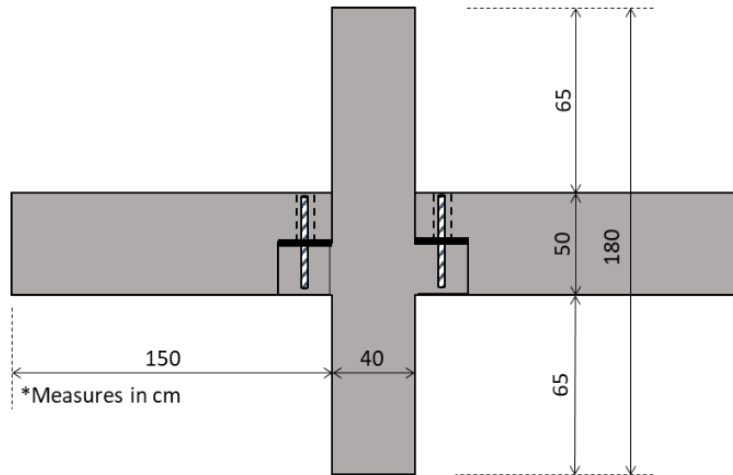

Figure 2. Basic model analyzed.

The characteristics of the connection were changed based on the basic model, assigning components that can increase the stiffness at the bending moment, such as anchoring the anchor, using a modified mortar pad (MMP), and filling the beam-column interfaces with grout. A summary of the models and their characteristics can be seen in Table 1 and Figure 3.

Table 1. Model characteristics.

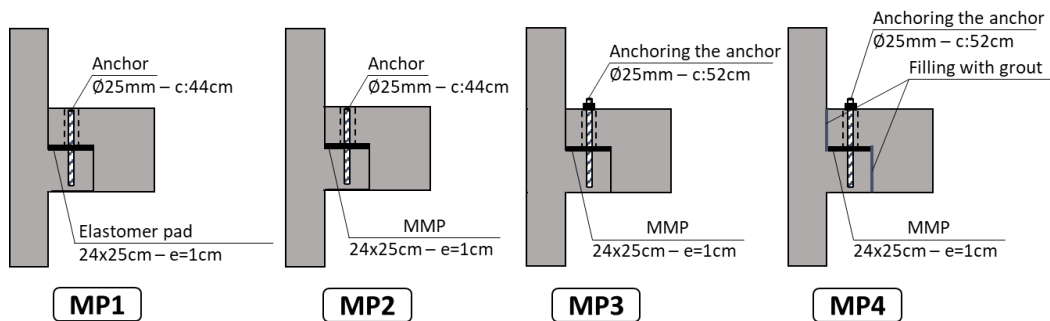| Characteristics	Connection model			
	MP1	**MP2**	**MP3**	**MP4**
Bearing pad	Elastomer	MMP	MMP	MMP
Anchoring the anchor to the top of the beam	✗	✗	✔	✔
Filling beam-column interfaces	✗	✗	✗	✔

Figure 3. Connection models analyzed.

To analyze the behavior of the connections, the following variables were evaluated: moment-rotation curve, cracking and ultimate moments, and failure mode.

3 NUMERICAL ANALYSIS

The numerical analysis was performed using the computer program ABAQUS®, version 6.12, based on the Finite Element Method which allows the analysis of several engineering problems. All its theoretical foundation is described in the Abaqus Theory Manual prepared by Dassault Systèmes S.A [9].

In the analyses, physical and geometric nonlinearities were considered, as well as the contact between surfaces. The models were discretized into two types of finite elements available in the ABAQUS® library. In all solid parts, C3D8 tetrahedral continuous elements were used, which are three-dimensional elements with 8 nodes. The reinforcements were modeled as bars, using the T3D2 element with 2 nodes; however, the continuity reinforcements of the calibration model and the half-joint and corbel tie rods of all models were modeled as solid, using the C3D8 element.

Load increments were performed using steps with automatic size adjustment based on computational efficiency but limited to the maximum increment of 1.0 kN. The Newton-Raphson method was used to solve the nonlinear problem.

3.1 Materials

All mechanical parameters of material characteristics were based on the experimental characterization tests described in Miotto [8]. For concrete modeling, the constitutive model Concrete Damaged Plasticity (CDP) was used, based on the Theory of Plasticity and Continuum Damage Mechanics, initially proposed by Lubliner et al. [10]. This model assumes that concrete has two failure mechanisms - cracking in tension and crushing in compression. The evolution of the failure surfaces is controlled by two variables $\tilde{\varepsilon}_t^{pl}$ (equivalent plastic strain in tension) and $\tilde{\varepsilon}_c^{pl}$ (equivalent plastic strain in compression).

In Miotto's experimental model [8], two concretes with different characteristics were used: one used for beams and column, and the other for filling the topping. The mechanical characteristics used in the modeling were: mean compressive strength (f_c), mean tensile strength (f_t), tangent modulus of elasticity (E_c), and Poisson's ratio (v_c), which are shown in Table 2.

Table 2. Mechanical characteristics of concretes

	Beams and column	Topping
Compressive strength (f_c)	49.0 MPa	33.2 MPa
Tensile strength (f_t)	3.2 MPa	2.9 MPa
Modulus of elasticity (E_c)	32.8 MPa	31.6 MPa
Poisson's ratio (v_c)	0.2	0.2

As Miotto [8] did not present the stress versus strain curves of the concretes used, data from Table 2 were extrapolated. To determine the stress versus strain curve of concrete under compression, the relationship proposed by Saenz [11] and modified by Hu and Schnobrich [12] was used, according to Equation 1 and which can be seen in Figure 4. For tension, the model used was the one proposed by Nayal & Rasheed [13] with the modifications from Wahalathantri et al. [14], as can be seen in Figure 5.

$$\sigma = \frac{E_c \varepsilon}{1 + \left(R + R_E - 2\right)\left(\dfrac{\varepsilon}{\varepsilon_0}\right) - \left(2R - 1\right)\left(\dfrac{\varepsilon}{\varepsilon_0}\right)^2 + R\left(\dfrac{\varepsilon}{\varepsilon_0}\right)^3} \tag{1}$$

Where: ε_0: Strain corresponding to peak stress and adopted as 0.0025;

ε_u: Ultimate strain adopted with $4\varepsilon_0$ according to Hu and Schnobrich [12];

f_u: Ultimate stress adopted with $f_c/4$ according to Hu and Schnobrich [12];

E_0: Secant modulus of elasticity (f_c / ε_0);

R_E: Relationship between tangent and secant modulus of elasticity (E_c / E_0);

R_ε: Strain rate ($\varepsilon_u / \varepsilon_0$), adopted as 4 according to Hu and Schnobrich [12];

R_σ: Stress ratio (f_c / f_u), adopted as 4 according to Hu and Schnobrich [12];

$$R = \left(R_E \left(R_\sigma - 1 \right) / \left(R_\varepsilon - 1 \right)^2 \right) - \left(1 / R_E \right).$$
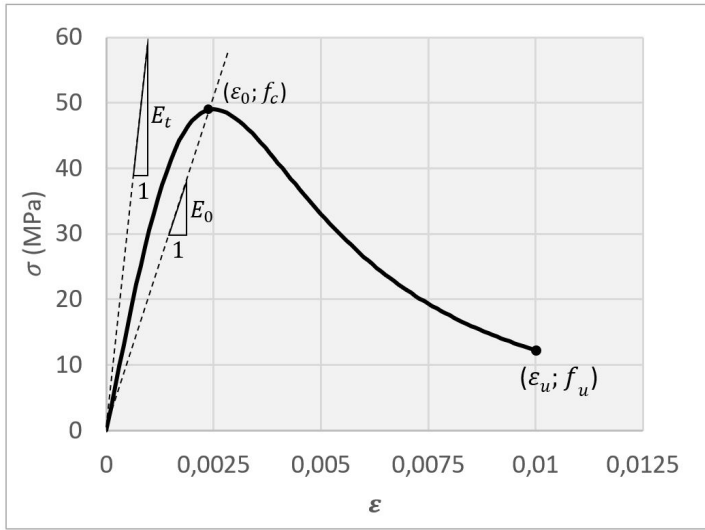
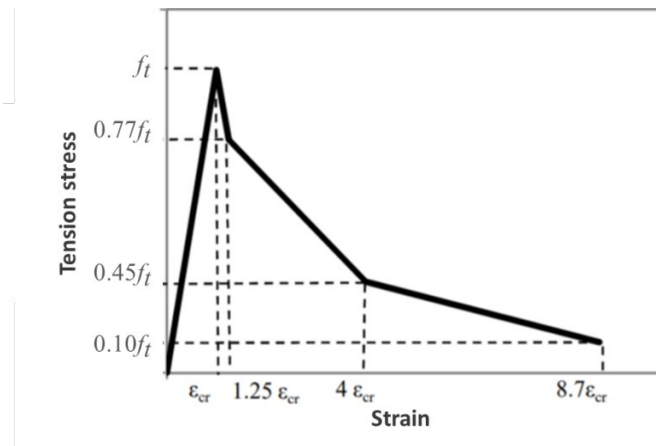**Figure 4.** Stress versus strain curve to uniaxial compression adopted for the model. (From the author)

Figure 5. Constitutive relation for concrete (Adapted from Wahalathantri et al. [14]).

The reinforcement and anchor steels were modeled with perfect elastoplastic behavior. For reinforcement, CA 50 steel was used and for anchor bolts, SAE 1020 steel was used. The yield stresses of the steels were obtained experimentally in Miotto [8], as well as the modulus of elasticity of steel SAE 1020, whereas the modulus of elasticity of steel CA 50 was adopted with a value of 200 GPa. The mechanical characteristics of steels can be seen in Table 3.

Table 3. Mechanical characteristics of steels

Type	Diameter (mm)	Yield stress (f_y) (MPa)	Modulus of elasticity (E_s) (GPa)
CA 50	10.0	576	200*
	12.5	611	200*
	16.0	589	200*
SAE 1020	-	576	201

*Values adopted due to the absence of experimental data

Rev. IBRACON Estrut. Mater., vol. 14, no. 5, e14505, 2021

5/17

In the calibration model, the bearing pad was made in modified mortar. This material has been researched in recent years (Ditz et al. [15], El Debs and Bellucio [16], Siqueira and El Debs [17]), in search of a composite that has a low modulus of elasticity, good mechanical resistance, and high tenacity. In this analysis, this material was modeled with elastic-linear behavior, using pad stiffness of 150 MPa.

In Model MP1, the material used in the pad was polychloroprene (Neoprene), a material widely used in elastomeric bearing pads by Brazilian manufacturers of precast structures. In this analysis, Neoprene was modeled with elastic-linear behavior and the relation proposed by Ferreira was used to determine the slab stiffness of this material [18], according to Equation 2.

$$E_n = K_1 GB + K_2 \sigma_m \tag{2}$$

Where: E_n : Slab stiffness (MPa);

K_1 and K_2 : Adjustment coefficients, adopted as 7 and 6 for Concrete-Neoprene contact surfaces, respectively;

G : Transverse modulus of elasticity (1.0 MPa);

σ_m : Average compression stress (5 MPa);

B : Form factor, given by Equation 3.

$$B = \frac{a\,b}{2h_n\,(a+b)} \tag{3}$$

Where: a and b : Plan dimensions of the pad;

h_n : Pad thickness.

The stiffness obtained by Equation 2 for Neoprene is approximately 73 MPa, which is consistent with the experimental results obtained in Montedor [19]. The filling grout was modeled with elastic-linear behavior, with a modulus of elasticity E_c of 4.94 GPa, according to experimental characterization tests performed by Miotto [8].

3.2 Contact

The models used in this analysis show several regions of interaction between surfaces, among them: the contact between the beam and column concrete and the bearing pad, the contact between the anchor and the surrounding concrete, and the contact between concrete surfaces of different ages.

Different tools available in ABAQUS® were used, which allowed the modeling of all regions of mechanical contact of the models. Basically, the embedded tool was used to simulate the relation between the reinforcement and the concrete, as well as the anchor and the concrete of the column. The tie constraint was used for the relation between concrete surfaces of different ages, as this constraint allows the nodes of a pair of surfaces to remain tied throughout the simulation; that is, all the translation and rotation movements of the nodes close to the two surfaces are equal.

For several interactions between surfaces, a possible relative sliding was considered, and the Coulomb Frictional Model was used. It is considered that two adjacent surfaces can transmit shear stresses up to a certain magnitude before relative sliding (adhesion) occurs. The stress which starts the relative sliding is given as a fraction of the contact pressure (p) and called critical stress (τ_{crit}) determined according to Equation 4. From the critical shear stress, there is a relative sliding between the surfaces as shown in Figure 6.

$$\tau_{crit} = \mu\,p \tag{4}$$

Where: μ : Coefficient of friction;
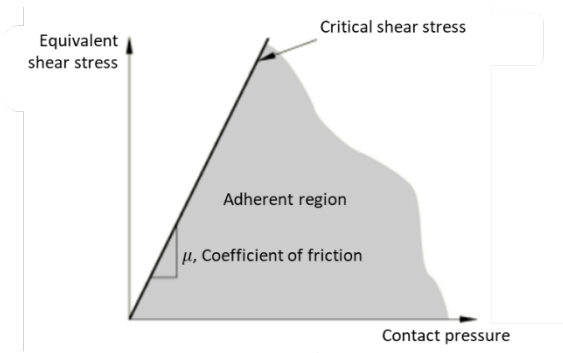
p : Contact pressure between surfaces.

Figure 6. Sliding conditions between surfaces in contact (adapted from Dassault Systèmes S. A. [9]).

The friction coefficients considered between the different surfaces were determined according to Miotto [8], Ferreira [18], and Magliulo et al. [20]. For contact surfaces between precast concrete, a friction coefficient of 0.6 was considered. For the contact between the steel of the SAE 1020 anchor (smooth) and the surrounding concrete (grout), a coefficient of $\mu = 0.01$ was considered. For the contact between concrete and the modified mortar pad, the value adopted for the friction coefficient was 0.4.

For the contact between the elastomeric bearing pad and the column and beam concrete, the relation proposed by Magliulo et al. [20], represented in Equation 5, was used. In this case, the coefficient of friction between concrete and Neoprene depends on the contact pressure between surfaces.

$$\mu = 0.49 \, if \, \sigma_p \leq 0.14 \, MPa$$

$$\mu = 0.1 + \frac{0.055}{\sigma_p} if \, 0.14 < \sigma_p \leq 5 \, MPa \tag{5}$$

Where: μ: Coefficient of friction;

σ_p: Average contact stress in the bearing pad.

For the consideration of the contact pressures between surfaces, this modeling used the hard relation of the program. Such relation considers that when surfaces are in contact, any stress is transmitted; however, when there is no contact between surfaces, there is no stress transmission, thus, surfaces that are initially separated are considered in contact when the separation distance between they are reduced to zero; from that moment, restrictions are imposed on the degrees of freedom of the nodes that form the surfaces and the stresses transmitted between them. This analysis is performed automatically by ABAQUS® between the surfaces previously defined and characterized by the user.

This modeling considered the contact formulation called surface pairs, in which the user can specify aspects of discretization, tracking approach, etc., specifically using the contact discretization called surface-to-surface that performs the analyses in average regions from the individual nodes of the surface.

4 CALIBRATION MODEL

Since the calibration model has symmetry in relation to two planes, the conditions of symmetry were used for the modeling, with the numerical model corresponding to 25% of the experimental structure, which allows the analysis to be performed at a lower computational cost. Symmetry was defined in the directions of the x and z axes, according to Figure 7. The boundary conditions were performed by setting the lower end of the column and applying stress to the beam end, as can be seen in Figure 7a. Figure 7b shows the reinforcement of the numerical model.

In this model, a total of 16136 C3D8 elements and 5580 T3D2 elements were used. The dimensions of the elements were varied and defined according to the degree of accuracy of the desired response.
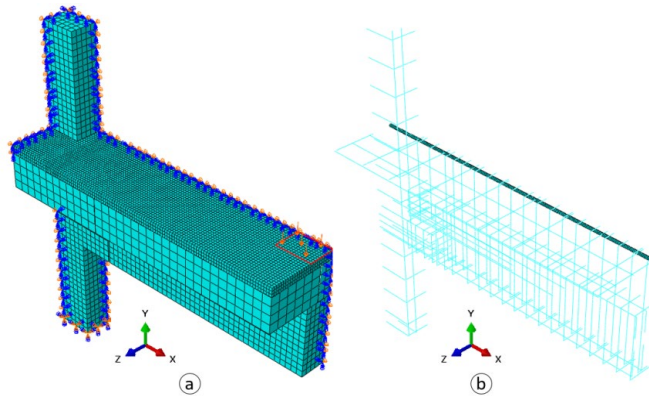
Rev. IBRACON Estrut. Mater., vol. 14, no. 5, e14505, 2021

7/17

Figure 7. Boundary conditions of the calibration model.

4.1 Moment-rotation curve and cracking and ultimate moments

The numerical model exhibited a behavior like the experimental model both for rotational stiffness and the cracking and failure moments. The experimental model was also numerically analyzed by Miotto [8] using the computer program ANSYS®, version 5.5. Figure 8 shows the development of the moment-rotation curve for the negative bending moment of the experimental and numerical model by Miotto [8] that was carried out in this research using ABAQUS®, version 6.12.

Both the numerical model and the experimental model exhibit three well-defined stiffness stages. The numerical model showed high indexes of initial stiffness until -39.67 kNm, when the cracking of the connection occurs. From this stage on, the connection presents a sharp drop in stiffness, which remains constant until the bending moment of approximately -233.75 kNm, considered the ultimate moment of the connection. The comparison of the cracking and ultimate moments of the experimental and numerical models can be seen in Table 4.

The numerical model did not exhibit the same rhythm of loss of stiffness as the experimental model in the second stage, mainly from the bending moment of -125 kNm. This difference in behavior may be attributed to the modeling of the modified mortar bearing pad and grout with elastic-linear behavior.
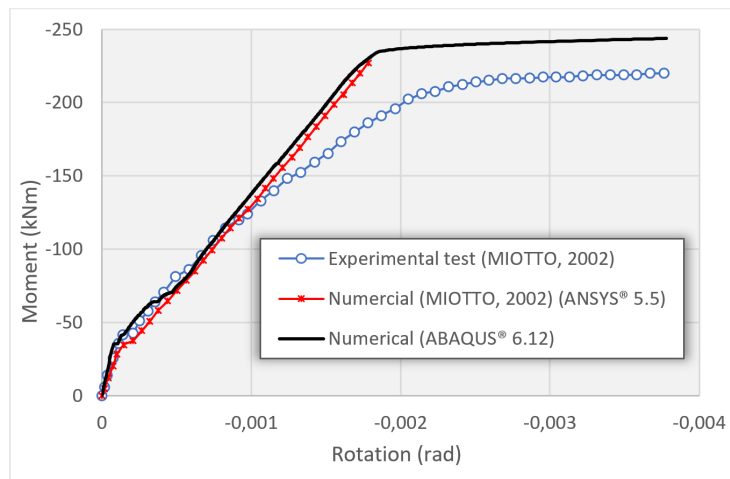

Figure 8. Moment-rotation curve of calibration model (Adapted from Miotto [8]).

Table 4. Comparisons of numerical and experimental bending moments

Model	Cracking moment (M_f) (kNm)	$\dfrac{M_{f,exp}}{M_{f,num}}$	Ultimate moment (M_u) (kNm)	$\dfrac{M_{u,exp}}{M_{u,num}}$
Experimental (Miotto [8])	-42.00		-220.75	
Numerical (ABAQUS 6.12)	-39.67	1.059	-233.75	0.944

Rev. IBRACON Estrut. Mater., vol. 14, no. 5, e14505, 2021

8/17

4.2 Cracking pattern and failure mode

Both the numerical model and the experimental model showed failure from the yield of the continuity reinforcement present in the concrete topping. In both cases, the models showed intense cracking on the topping from the strain of the reinforcement. To analyze the cracking of the numerical model, the distribution of plastic deformations was verified, which indicates the occurrence of cracks in the concrete with certain accuracy.

Figure 9 shows the distribution of plastic deformations in the concrete of the numerical model and a diagram of the distribution of cracks in the experimental reference model for their respective ultimate moments. There is a good relation between the cracking patterns of the numerical model and the experimental model.

Miotto [8] mentions that cracks started near the column and were moving away to the external regions. This configuration was similar in the numerical model, in which the first crack occurred precisely in the protruding corner of the column. After the first crack, there were other cracks close to the region of symmetry, and with the increase of the acting moment, parallel cracks formed towards the load application region at the end of the beams.
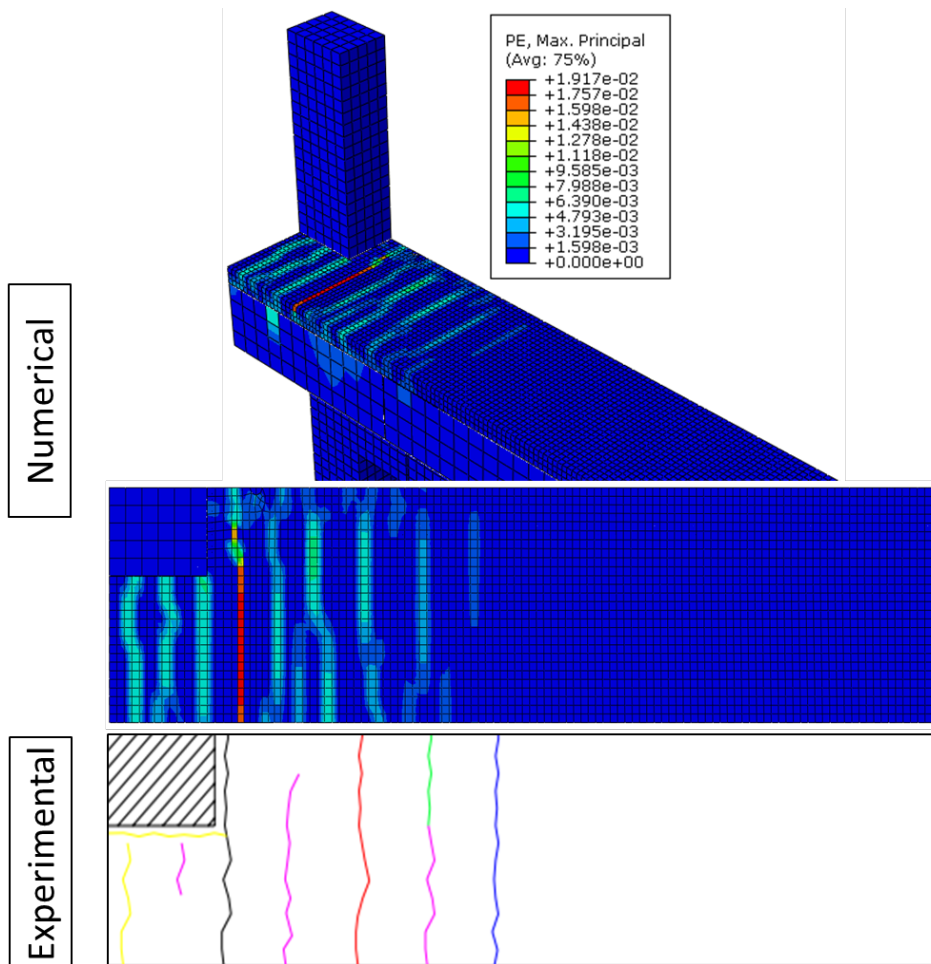

Figure 9. Comparison of the cracking pattern of the models. (Adapted from Miotto [8]).

5 NUMERICAL MODELS

With the good convergence of the behavior of the calibration model, the extrapolated models shown in Figure 3 could be analyzed. The results are presented in the following items.

The number of finite elements used in the models can be seen in Table 5. The boundary conditions were defined in a similar way to the calibration model and Figure 10 shows the numerical models.

Table 5. Number of finite elements of the numerical models

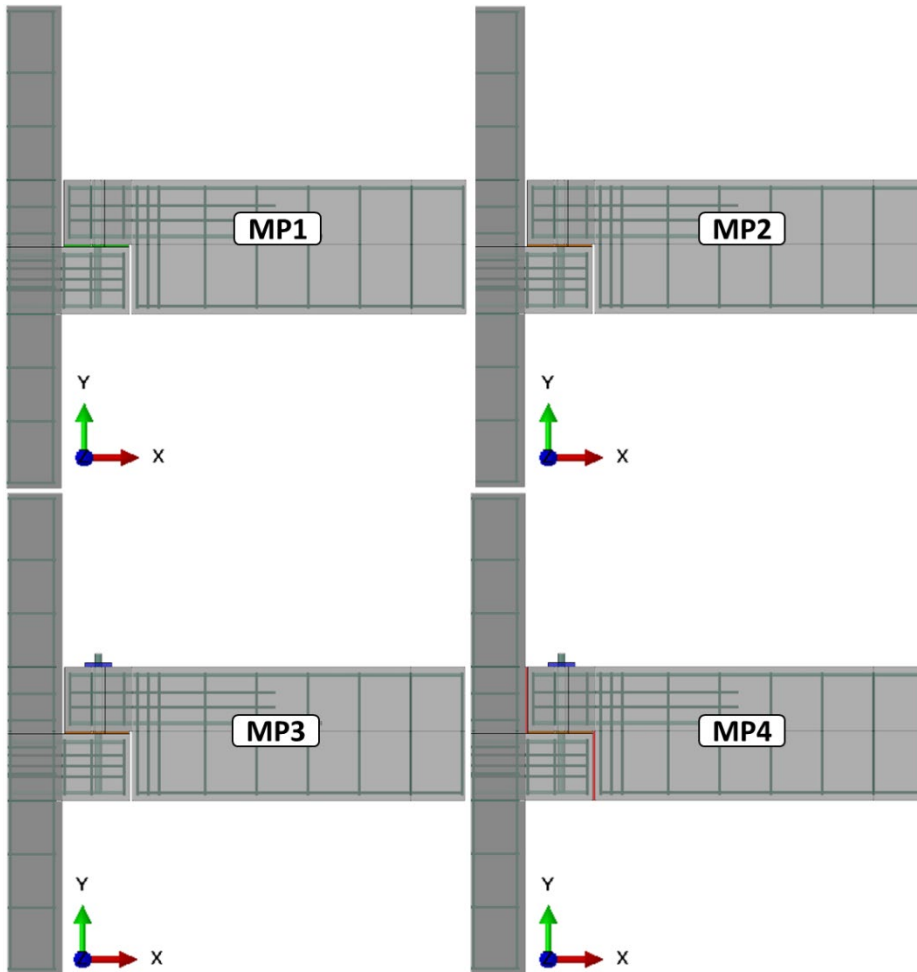| Model	Number of elements	
	C3D8	T3D2
MP1	8559	2403
MP2	8559	2403
MP3	8811	2403
MP4	9474	2403

Figure 10. Numerical models.

The calculation of the reinforcements and the verification of the concrete in the corbels and half-joints of the models were made according to the calculation model indicated by the Brazilian technical standard NBR 9062 [21] for corbels and are composed of main reinforcement (tie rods) and secondary reinforcements that include horizontal and vertical stirrups and suspension reinforcement exclusively for the half-joint.

5.1 Moment-rotation curve

The moment-rotation curve of the models was determined similarly to the calibration model, by checking the relative horizontal displacement of the beam at the vertical joint near the column. The secant stiffness was determined when the yield of the anchor of the connections began, as well as its initial tangent stiffness. These curves were determined for all models and are shown below.

It is worth mentioning that the curves shown in Figures 12, 13, and 14 do not show the complete behavior of the models MP1, MP2 and MP3, since the part of the behavior that occurs after contact between the lower part of the corbel and the lower part of the half-joint was suppressed according to Figure 11.
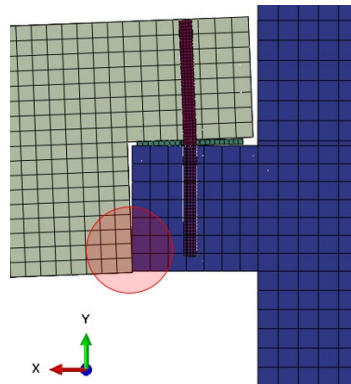
Figure 11. Contact between the half-joint and the corbel.

5.1.1 MP1

The only mechanism of resistance to rotation presented by the connection of model MP1 is the anchor subjected to bending by the pin effect; therefore, the model exhibits low initial tangent stiffness, with a value of 569.15 kNm/rad. This result can also be attributed to the low stiffness of the bearing pad, which in this model consists of polychloroprene (Neoprene). The moment-rotation curve of model MP1 can be seen in Figure 12. The moment that characterizes the beginning of the yield of the anchor was approximately -9.33 kNm and was obtained by monitoring the development of the main stresses in the anchor as the bending moment increments occurred.
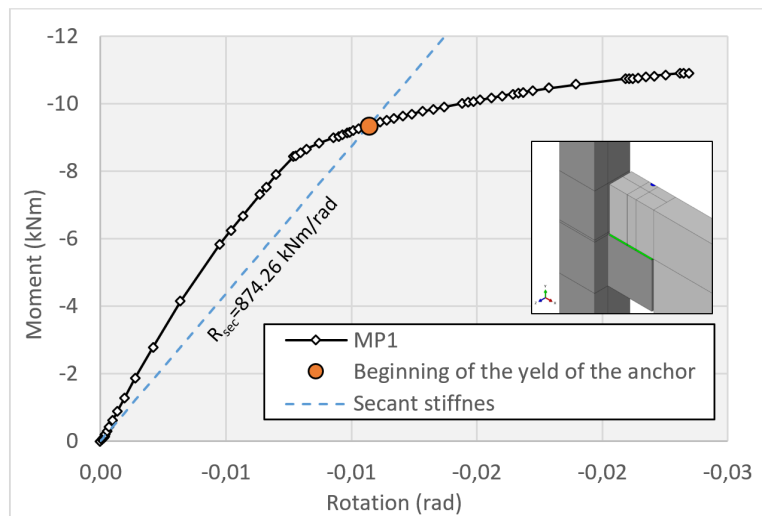
Figure 12. MP1 moment-rotation curve.

5.1.2 MP2

The only change in model MP2 is the use of a modified mortar pad in place of the elastomer. The model exhibits an initial tangent stiffness greater than MP1, with a value of 956.43 kNm/rad. The moment-rotation curve of model MP2 can be seen in Figure 13.
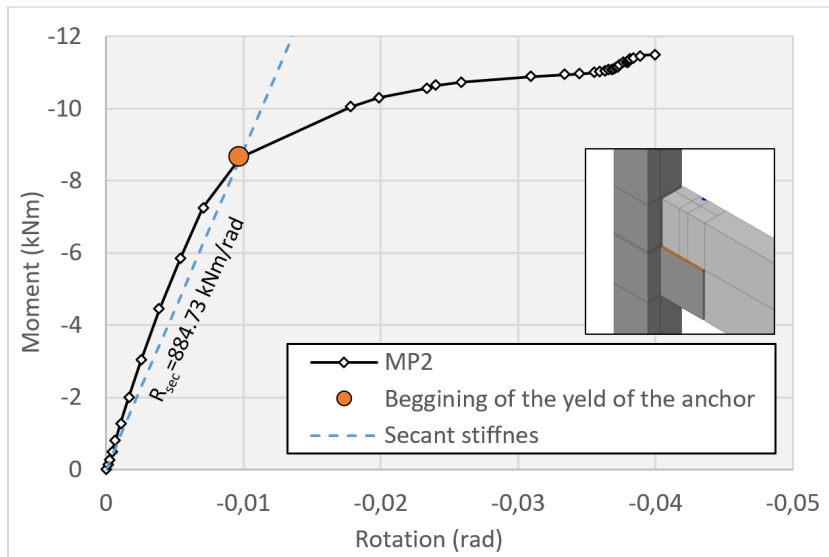
Figure 13. MP2 moment-rotation curve.

5.1.3 MP3

As shown in Figure 14, the anchoring of the anchor to the top of the beam changed the behavior of the connection, causing the moment-rotation curve not to show a marked drop in stiffness as in models MP1 and MP2. This is because with the anchoring the anchor is no longer mainly required by the bending, due to the pin effect, and it is also subjected to tension. This effect can be observed through the distribution and direction of the main stresses in the anchors of models MP2 and MP3 according to Figure 15, in the contact between the corbel and the half-joint.

It can be seen in Figure 15 that the anchor of model MP2 exhibits a concentration of stresses greater than 600 MPa both in tension and compression near the turning point of the connection (pin effect) forming a plastic hinge, while in model MP3 there is a distribution of more uniform tensile stresses along the anchor with values of approximately 500 MPa; it can also be observed that the stress directions in the anchor of model MP3 are almost entirely of axial tension, differently from the anchor of model MP2.

Another important factor for the more linear behavior of the moment-rotation curve of model MP3 is the fact that, in this case, virtually all the relative sliding that may occur between the anchor and the concrete surrounding the beam is practically eliminated from the anchoring of the anchor. The connection shows an initial tangent stiffness of 1081.27 kNm.
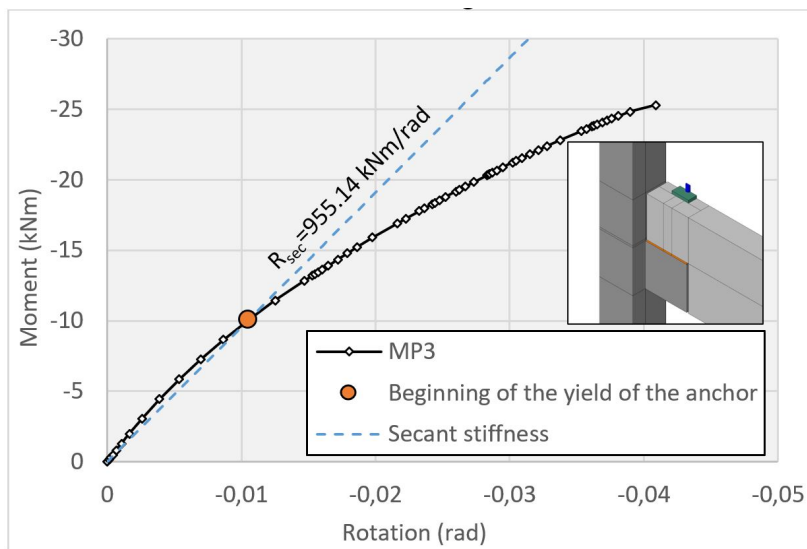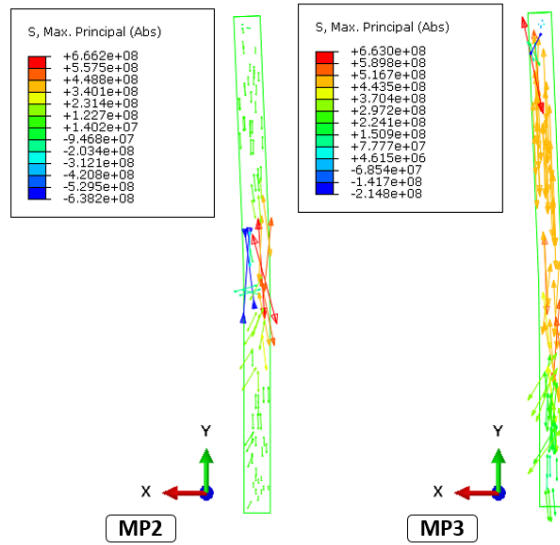

Figure 14. MP3 moment-rotation curve.

Rev. IBRACON Estrut. Mater., vol. 14, no. 5, e14505, 2021

12/17

Figure 15. Distribution and direction of the main stresses in the anchors of models MP2 and MP3 (Stresses in Pa).

5.1.4 MP4

Grout filling in model MP4 considerably increased the stiffness of the connection. Model MP4 exhibited an initial tangent stiffness of 12156.08 kNm, noticeably greater than the other models. Figure 16 shows that the stiffness in the connection of Model MP4 is higher and more resistant than in models MP1, MP2, and MP3.
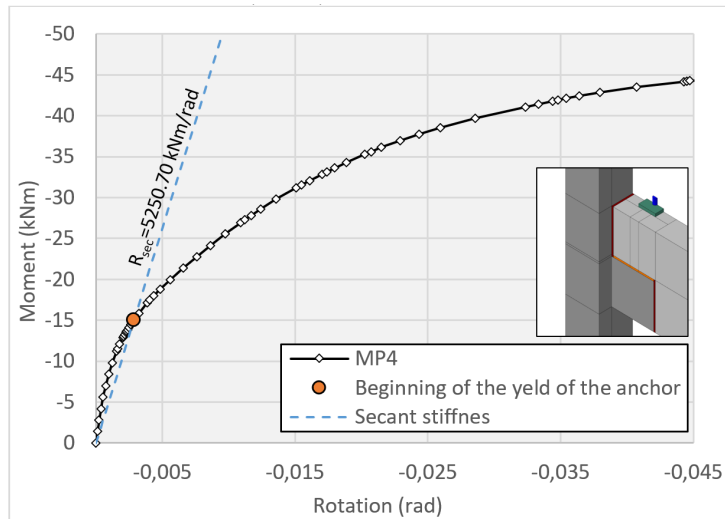

Figure 16. MP4 moment-rotation curve.

Figure 17 exhibits the complete moment-rotation curve of all models, showing an increase in the stiffness of models MP2 and MP3 after the beginning of the yield of the anchor, and this increase corresponds to the moment of contact between the corbel and half-joint.

5.2 Overview

Comparing the moment-rotation curves of all models in Figure 17, it appears that the initial behavior of models MP1, MP2, and MP3 is quite similar, and the only difference is that model MP3 does not show a sharp drop in stiffness as discussed in the previous paragraphs and shown in Figure 15.

J. V. M. A. Silva, L. Vanalli, L. A. F. Souza, and C. P. M. Rolim

The moments of the beginning of the yield of the anchors for models MP1, MP2, and MP3 are similar, as seen in Table 6, and this indicates that the changes proposed for these models were not effective to increase stiffness, not even the strength of the connections. On the other hand, the moment of the beginning of the yield of the anchor of model MP4 was 49.35% higher than for model MP3, which shows greater resistance ability.

Model MP4 also showed a considerably greater stiffness in relation to the other models, with its initial tangent stiffness 11.24 times greater than the stiffness of model MP3, and its secant stiffness at the beginning of the yield of the anchor was 5.5 times greater as shown in Table 7. This can be credited to the fact that the filling of the interfaces creates a resistance mechanism to the relative rotation between beam and column, limiting the strains in the compressed bottom because of the good resistance of the grout to compression and its high modulus of elasticity. However, in the upper region there is no type of tensile strength mechanism, since there is no considerable adherence between the filling grout and the concrete of the beam, thus making the anchor subjected to flexure-tension the fundamental element for resistance against the bending of the connection.
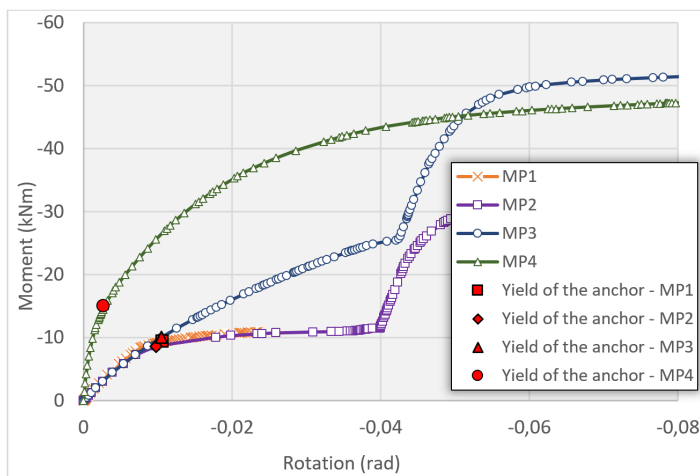

Figure 17. MP1, MP2, MP3, and MP4 moment-rotation curve.

Table 6. Model moments and rotations

Model	M_y (kNm)	Relative difference	M_u (kNm)	Relative difference
MP1	-9.33	-	-	-
MP2	-8.65	-7.29%	-32.43	-
MP3	-10.05	16.18%	-50.88	56.89%
MP4	-15.01	49.35%	-46.61	-6.59%
Model	θ_y (rad)	Relative difference	θ_u (rad)	Relative difference
MP1	0.0107	-	-	-
MP2	0.0098	-8.63%	0.0680	-
MP3	0.0105	7.62%	0.0610	-10.26%
MP4	0.0029	-72.83%	0.0680	11.48%

Table 7. Stiffness of models

	MP1	MP2		MP3		MP4	
	Stiffness (kNm/rad)	Stiffness (kNm/rad)	R_{MP2}/R_{MP1}	Stiffness (kNm/rad)	R_{MP3}/R_{MP2}	Stiffness (kNm/rad)	R_{MP4}/R_{MP3}
Initial (tangent)	569.15	1083.35	1.903	1081.27	0.998	12156.08	11.242
Yield of the anchor (secant)	874.26	884.73	1.012	955.14	1.080	5250.70	5.497

5.3 Failure mode

Model MP1 exhibited convergence problems, which can be attributed to the difficulty in modeling the contact relations between the concrete and the Neoprene pad. However, the connection already showed a well-established plastification of the anchor by the formation of a plastic hinge, which can be seen in Figure 18, and Figure 17 also shows that the MP1 and MP2 connection exhibit very similar behaviors except for initial tangent stiffness, which can be attributed to the difference in stiffness between the MMP and the polychloroprene pad, so that it can be said that the connections would exhibit similar behavior until failure. For the other models, the behavior could be observed at the ultimate moments.

All models presented plastification of the anchor from the bending caused by the pin effect in the region close to the bearing pad, forming a plastic hinge, as shown in Figure 18b. However, it is interesting to see that in models MP3 and MP4, the anchoring of the anchor to the upper part of the beam introduces tension effects to the anchor, as shown in Figure 15 and Figure 18.
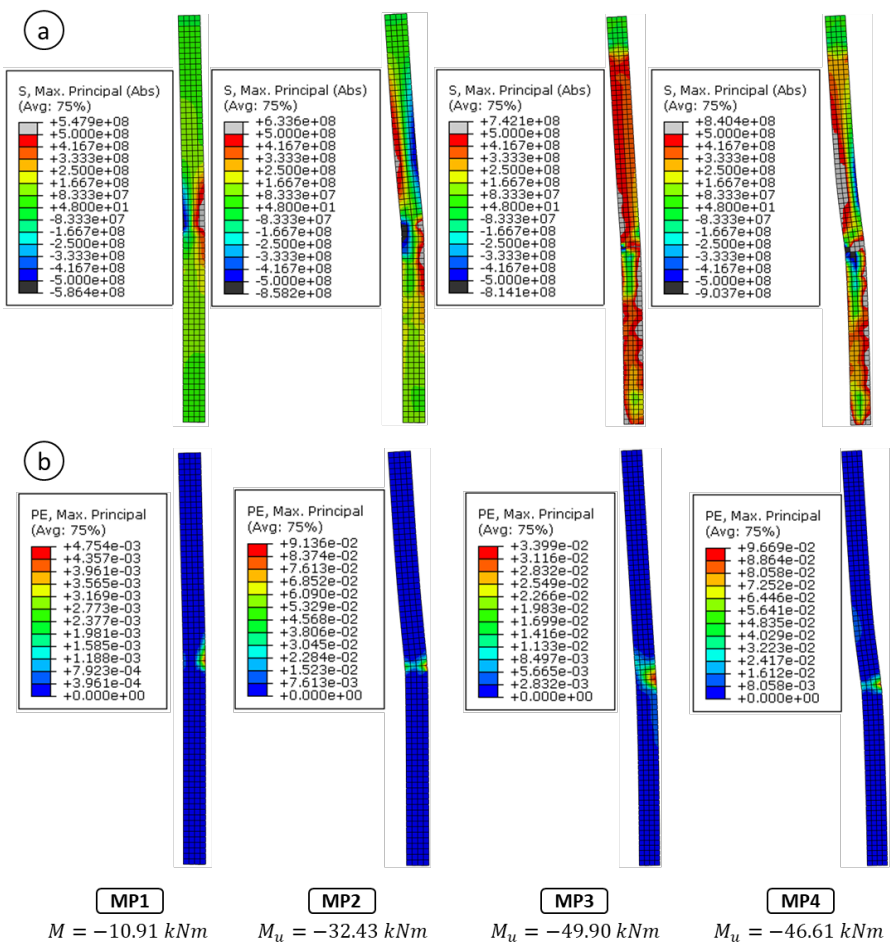

Figure 18. Anchors. a) Main maximum stresses; b) Main maximum strains. (Stresses in Pa).

The models had their ultimate moment reached mainly by the complete yield of the anchor; however, it is important to note that models MP3 and MP4 in their ultimate moment exhibit intense plastic strains in the corbel and in the half-joint. This is because in these models other mechanisms for transferring stresses are developed: (i) due to the anchoring of the anchor in the upper part of the beam, it compresses at the end of the upper side of the corbel in the region close to the half-joint thus causing plastic strains as shown in Figure 19; (ii) in model MP4, due to the filling of the interfaces, plasticization of the lower region of the corbel also occurs because of the compression caused by the negative bending moment.

We believe that the reason why model MP4 had lower ultimate resistance in relation to MP3, even though it exhibited greater M_y and stiffness, is precisely the introduction of the new mechanisms for transferring stresses. It is

important to note that these new mechanisms for transferring stresses are not considered in the corbel calculation model presented by NBR 9062 [21]; therefore, in these cases, a systematic analysis of the structural behavior of the connection is essential to perform a correct design.
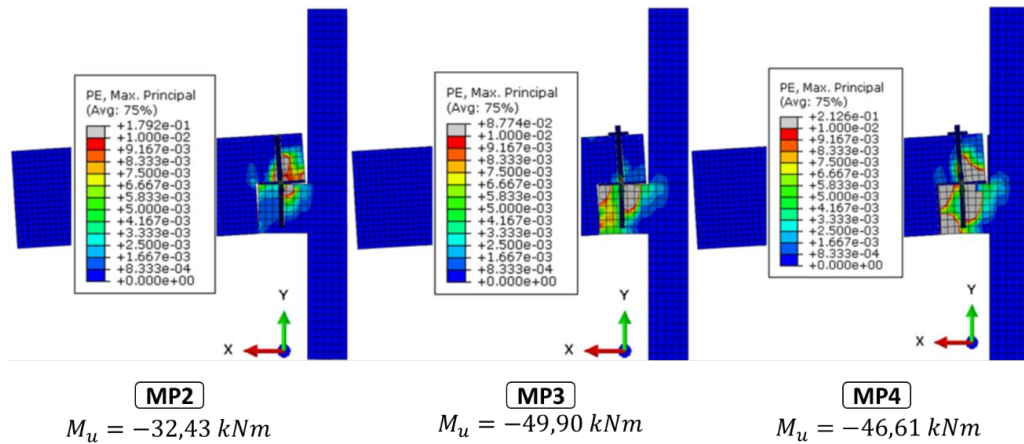

| **MP2** | **MP3** | **MP4** |
| $M_u = -32,43\ kNm$ | $M_u = -49,90\ kNm$ | $M_u = -46,61\ kNm$ |

Figure 19. Distribution of plastic strains for M_u.

6 CONCLUSIONS

In this research, the behavior of precast beam-column connections, without continuity reinforcement, subjected to negative bending moment was analyzed through numerical simulation in a computer program based on the Finite Element Method. The connection experimentally analyzed in Miotto [8] was modeled to obtain the calibration of the numerical analysis and thus perform the extrapolation to the other proposed models. With the good relation between the behavior of the numerical model and the experimental reference model, analyses could be carried out.

With the main objective of analyzing the behavior of precast beam-column connections, subjected to negative bending moment, without continuity reinforcement, and easily executed, four connection models with different characteristics were proposed to evaluate the influence of connection components in their behavior.

Replacing the elastomeric bearing pad by MMP generated a significant difference in the initial tangent stiffness of the connection, which was 90.35% greater in the model with MMP, which is attributed to the difference in stiffness between the modified mortar and the polychloroprene rubber. However, the moment of the beginning of the yield of the anchor and the secant stiffness of the connections showed similar values.

The anchoring of the anchor to the upper region of the connection increased its ultimate resistance, as the anchoring introduces tension effects to the anchor and decreases its bending at the height of the interface with the upper surface of the corbel. The anchoring also introduces a compressed region on the upper side of the corbel and close to the half-joint of the beam; however, it did not influence the initial stiffness of the connection, nor did it influence the moment of the beginning of the yield of the anchor.

The filling of the beam-column interface regions with grout generated quite positive effects, increasing the moment of the beginning of the plasticization of the anchor by 49% and the secant stiffness by 5.5 times.

Therefore, it is possible to conclude, through the analyses of the numerical models, that the filling of the interfaces with rigid material allows for the increased strength and stiffness of the connection. However, it is important to note that the use of this resource introduces new mechanisms for transferring stresses in the connection, which must be considered in its structural design.

There are benefits in considering the stiffness of this type of connection in precast single-storey or small height structures in the distribution of their stresses, which allows greater competitiveness of precast structures in relation to other structural systems.

In this context, future work should evaluate the behavior of connections without continuity reinforcement with filling the connection of the beam-column interface, to understand the stress distribution in the connection to propose structural calculation models, as well as the influence of its behavior in precast structures.

REFERENCES

[1] M. K. El Debs, *Concreto Pré-moldado: Fundamentos e Aplicações*, 2. ed. São Paulo: Oficina dos Textos, 2017.

[2] Kataoka, M. N., Ferreira, M. A., and El Debs, A. L. H. C., "A study on the behavior of beam-column connections in precast concrete structures: experimental analysis," *Rev. IBRACON Estrut. Mater.*, vol. 5, no. 5, pp. 848–873, 2012.

[3] Lacerda, M. M. S. et al. "Influence of the vertical grouting in the interface between corbel and beam in beam-to-column connections of precast concrete structures – An experimental analysis," *Eng. Struct.*, vol. 172, pp. 201–213, Maio 2018. https://doi.org/10.1016/j.engstruct.2018.05.113

[4] A. Baldissera Estudo experimental de uma ligação viga-pilar de concreto pré-moldado parcialmente resistente a momento fletor. Universidade de São Paulo, 2006.

[5] M. K. El Debs, A. M. Miotto, and A. L. H. C. El Debs, "Analysis of a semi-rigid connection for precast concrete," *Proc. Inst. Civ. Eng., Struct. Build.*, vol. 163, no. 1, pp. 41–51, 2010. Accessed: Oct. 12, 2018. [Online]. Available: http://www.icevirtuallibrary.com/doi/10.1680/stbu.2009.163.1.41

[6] L. A. Oliveira Júnior et al., "Precast beam–column connection subjected to cyclic and dynamic loadings," *Struct. Eng. Int.*, vol. 27, no. 1, pp. 114–126, 2017. Accessed: Oct. 12, 2018. [Online]. Available: http://www.ingentaconnect.com/content/10.2749/101686617X14676303589075

[7] F. Y. Sawasaki, "Estudo teórico-experimental de ligação viga-pilar com almofada de argamassa e chumbador para estruturas de concreto pré-moldado," Master thesis, Univ. S. Paulo, São Carlos, SP, 2010.

[8] A. M. Miotto, "Ligações viga-pilar de estruturas de concreto pré-moldado análise com ênfase na deformabilidade ao momento fletor," Doctoral dissertation, Univ. S. Paulo, São Carlos, SP, 2002.

[9] Dassault Systèmes, *ABAQUS 6.12*. Documentation. French: Dassault Systèmes, 2012.

[10] J. Lubliner et al., "A plastic-damage model for concrete," *Int. J. Solids Struct.*, vol. 25, no. 3, pp. 299–326, 1989.

[11] L. P. Saenz, "Discussion of 'Equation for the stress–strain curve of concrete' by Desayi, P. and Krishnan, S.," *ACI Journal*, vol. 61, pp. 1229–1235, 1964.

[12] H.-T. Hu and W. C. Schnobrich, "Constitutive modeling of concrete by using nonassociated plasticity," *J. Mater. Civ. Eng.*, vol. 1, no. 4, pp. 199–216, 1990.

[13] R. Nayal and H. A. Rasheed, "Tension stiffening model for concrete beams reinforced with steel and FRP bars," *J. Mater. Civ. Eng.*, vol. 18, no. 6, pp. 831–841, 2006.

[14] B. L. Wahalathantri et al. "A material model for flexural crack simulation in reinforced concrete elements using ABAQUS," *Inf. Transp. Urban Develop.*, pp. 260–264, 2011.

[15] J. D. Ditz, M. K. E. L. Debs, and G. H. Siqueira, "Modified mortar pad behavior in the transfer of compressive stresses," *Rev. IBRACON Estrut. Mater.*, vol. 9, no. 3, 2016.

[16] M. K. El Debs and E. K. Bellucio, "Almofadas de apoio feitas de argamassa para ligações de concreto pré-moldado: estudo da rugosidade superficial," *Rev. IBRACON Estrut. Mater.*, vol. 5, no. 1, pp. 38–67, 2012.

[17] G. H. Siqueira, and M. K. El Debs, "Cement-based bearing pads for precast concrete connections," *Proc. Inst. Civ. Eng. – Const. Mater.*, vol. 166, no. 5, pp. 286–294, 2013. Accessed: Oct. 12, 2018. [Online]. Available: http://www.icevirtuallibrary.com/doi/10.1680/coma.11.00055

[18] M. A. Ferreira, "Deformabilidade de ligações viga-pilar de concreto pré-moldado," Doctoral dissertation, Univ. S. Paulo, São Carlos, SP, 1999.

[19] L. C. Montedor, "Desenvolvimento de compósito a ser utilizado como almofada de apoio nas ligações entre elementos pré-moldados," Master thesis, Univ. S. Paulo, São Carlos, SP, 2004.

[20]   G. Magliulo et al., "Neoprene-concrete friction relationships for seismic assessment of existing precast buildings," *Engineering Structures*, vol. 33, no. 2, pp. 535–538, 2011. http://dx.doi.org/10.1016/j.engstruct.2010.11.011

[21] Associação Brasileira de Normas Técnicas. *Projeto e Execução de Estruturas de Concreto Pré-moldado*, NBR 9062, 2017.

Rev. IBRACON Estrut. Mater., vol. 14, no. 5, e14505, 2021

17/17